Benchmarking of the NCrystal SANS Plugin for Nanodiamonds

Rizzi, Nicola; Marquez Damian, Jose I.; Kittelmann, Thomas; Lauritzen, Bent; Klinkby, Esben; Estiez, Quentin; Santoro, Valentina

Published in:
Nuclear Science and Engineering

Link to article, DOI:
10.1080/00295639.2023.2196926

Publication date:
2024

Document Version
Publisher's PDF, also known as Version of record

Nuclear Science and Engineering

ISSN: (Print) (Online) Journal homepage: https://www.tandfonline.com/loi/unse20

Benchmarking of the NCrystal SANS Plugin for Nanodiamonds

Nicola Rizzi, Jose I. Marquez Damian, Thomas Kittelmann, Bent Lauritzen, Esben Klinkby, Quentin Estiez & Valentina Santoro

To cite this article: Nicola Rizzi, Jose I. Marquez Damian, Thomas Kittelmann, Bent Lauritzen, Esben Klinkby, Quentin Estiez & Valentina Santoro (27 Apr 2023): Benchmarking of the NCrystal SANS Plugin for Nanodiamonds, Nuclear Science and Engineering, DOI: 10.1080/00295639.2023.2196926

To link to this article: https://doi.org/10.1080/00295639.2023.2196926

Published online: 27 Apr 2023.

NUCLEAR SCIENCE AND ENGINEERING

DOI: https://doi.org/10.1080/00295639.2023.2196926

Benchmarking of the NCrystal SANS Plugin for Nanodiamonds

Nicola Rizzi,[a]* Jose I. Marquez Damian,[b] Thomas Kittelmann,[b] Bent Lauritzen,[a] Esben Klinkby,[a,b] Quentin Estiez,[c] and Valentina Santoro[b]

[a]*Technical University of Denmark, Department of Physics, Risø, Denmark*
[b]*European Spallation Source ERIC, Lund, Sweden*
[c]*UGA Graduate School of Engineering in Physics, Electronics, Materials Sciences, Grenoble INP – Phelma, 3 Parvis Louis Neel – CS 50257 – 38016 Grenoble Cedex 1, France*

Received November 21, 2022
Accepted for Publication March 25, 2023

Abstract — *Nanodiamonds have attracted attention in recent years for their exceptional albedo of slow neutrons. Several theoretical models have been proposed to compute the total elastic cross section. However, these models neglect the relatively complex internal structure and chemical composition of the diamond nanoparticles, relying often on the monodisperse structureless spheres approximation. In this work, we explore the possibility of adding the small-angle neutron scattering (SANS) process for nanodiamonds to NCrystal, a library that enables calculations for Monte Carlo simulations of neutrons in polycrystalline materials and powders. This approach aims to describe the scattering process also at neutron wavelengths below the diamond Bragg cutoff where simple models usually struggle. The extension relies on modeling the SANS process through the fitting of experimental data as well as theoretical inputs. The code can then be coupled with an existing simulation framework, such as McStas, and benchmarked in different setups. We tested the plugin for two properties of diamond powder nanoparticles: the backward reflection of very cold neutrons and the quasispecular reflections of cold neutrons. The validation of this simulation tool is intended to pave the way for the design of the beam extraction system for a future high-intensity cold neutron moderator at the European Spallation Source.*

Keywords — *Nanodiamonds, very cold neutrons, reflectivity, NCrystal, McStas.*

Note — *Some figures may be in color only in the electronic version.*

I. INTRODUCTION

Nanodiamonds (NDs), with exceptionally high very cold neutron (VCN) albedo[1] (diffuse reflectivity at all incidence angles) and cold neutron (CN) quasispecular reflectivity at small angles, are a candidate to fill the so-called energy gap in reflectors for CNs and VCNs (Ref. 2). Since NDs represent a particularly promising material for the design of beam extraction systems for CN and VCN sources, there is great interest in the measurement of ND neutron scattering cross sections,[3–5] as well as in their implementation in neutronic simulations codes.[5–7]

From a theoretical point of view, the outstanding performance of NDs is mainly due to the large coherent scattering cross section (5.55 b at standard thermal energy) associated with both low absorption (3.5 mb at standard thermal energy) and low inelastic scattering. Moreover, ND powders with nanoparticles of an average size of 4 to 5 nm obtained from detonation[8] (DND) are currently available on an industrial scale, which makes them a suitable choice for the production of real full-sized

*Email: nicri@dtu.dk

neutron reflectors. Some challenges in the use of DNDs lie in the possibility of both hydrogenous contamination on the nanoparticle surface, which causes neutron losses, or upscattering to thermal energies[9] and clustering, which is the close packing of neighboring DNDs; both of which have the effect of reducing the overall reflection efficiency.[10]

Theoretical models have already been proposed to compute the total elastic cross section.[5,11] However, these models are limited by the structureless sphere approximation (mono or polydisperse), which neglects the complex internal structure of NDs. In this work, we seek to overcome this limitation by adding the small-angle neutron scattering (SANS) process to the NCrystal libraries[12] for elastic and inelastic bulk physics, with the aim to describe neutron scattering also at neutron wavelengths below the diamond Bragg cutoff, where simple models are insufficient.

This plugin extends the simulation potential of the library by modeling SANS through both the empirical models, i.e., fitting existing experimental data, and the theoretical models. The possibility of loading experimental data directly also has been implemented, allowing users to plug in their own SANS measurements of a particular ND sample. The code (available at Ref. 13) is coupled to the McStas simulation framework[14] and has been benchmarked in different setups. We test the plugin for two aspects of ND scattering: the backward reflection of VCNs and the quasispecular reflections of CNs. The validation of this simulation tool is intended to pave the way for the design of a beam extraction system for the high-intensity CN and VCN sources at the European Spallation Source (ESS).

We introduce in Secs. II and III the empirical and theoretical models used to fit the experimental $I(q)$, with q being the usual notation for the scattering vector and $I(q)$ the differential microscopic cross section $\frac{d\sigma}{d\Omega}(q)$. In Sec. IV, we give an overview of the implementation. Finally, we show the validation of the code for the backward reflection of VCNs and quasispecular reflections of CNs in Sec. V.

II. EMPIRICAL MODELS

In this section, we present two analytical functions used to fit experimental $I(q)$ data: a piecewise power-law model and the more common Guinier-Porod parameterization. This approach was inspired by the work of Granada et al.[6,15] These empirical models are applied to the SANS $I(q)$ measured by Teshigawara et al.[3] It should be noted that these models are not intended to be an accurate microscopic description of the neutron interactions with matter, but more of an explanation of the observed behavior

II.A. Piecewise Power Law

In Ref. 6, the experimental data were fitted using the unified exponential/power-law approximation, as expressed in Eq. (3) in Ref. 16. Here we simplify the function into a piecewise power law:

$$I(q) = \begin{cases} A_1 q^{b_1} & q < Q_0 \\ A_2 q^{b_2} & q > Q_0 \end{cases} , \tag{1}$$

where b_i is the slope of the line in the log-log scale, Q_0 is the length of the scattering vector defining the boundary between the two regions, and A_i is a scaling factor that accounts also for boundary condition at Q_0. The results, along with the initial data, are shown in Fig. 1. The piecewise power-law approximation allows us to analytically compute the total SANS cross section with a closed-form expression,

$$\sigma(k_0) = \int I(q) d\Omega = \frac{2\pi}{k_0^2} \int_0^{2k_0} qI(q) \mathrm{d}q \ , \tag{2}$$

hence, Eq. (1) leads to

$$\begin{aligned} \sigma_{\mathrm{SANS}}(k_0) = & \ \frac{2\pi}{k_0^2} \left(\int_0^{Q_0} qI(q) dq + \int_{Q_0}^{2k_0} qI(q) dq \right) \\ = & \frac{2\pi}{k_0^2} \left[\frac{A_1}{b_1+2} Q_0^{b_1+2} + \frac{A_2}{b_2+2} (2k_0)^{b_2+2} - \frac{A_2}{b_2+2} Q_0^{b_2+2} \right] \end{aligned} , \tag{3}$$

where k_0 is the length of the incident wavevector.

II.B. Guinier-Porod Model

A widespread parametrization of the SANS absolute intensity is the Guinier-Porod profile,[17] which allows us to obtain the radius of gyration and the shape of the nanoparticles. To account for the increase of $I(q)$ in the very-low-q region, an additional power-law fit is added below Q_1, a user-specified boundary parameter:

$$I(q) = \begin{cases} Cq^{-p} & Q_{min} \le q \le Q_1 \\ q^{-s} \exp\left(\frac{-q^2 r_g^2}{3-s}\right) & Q_1 \le q < Q_2 \\ Bq^{-m} & q \ge Q_2 \end{cases} . \tag{4}$$

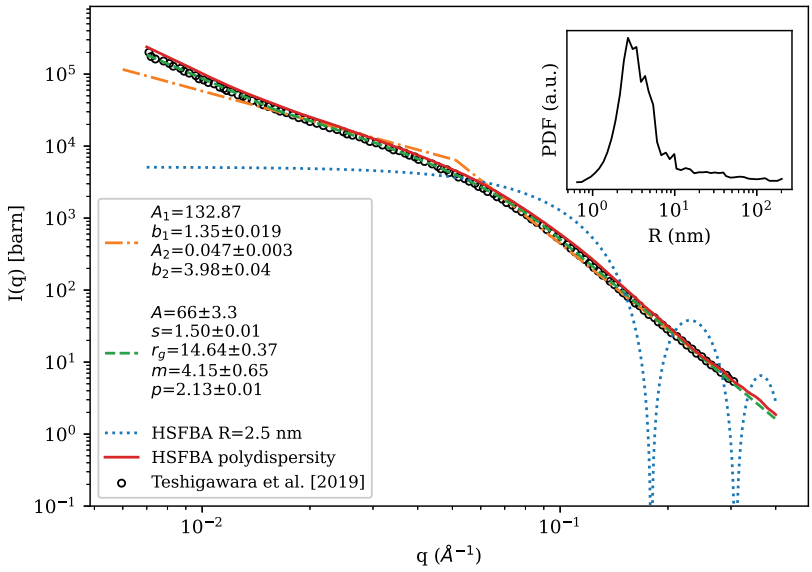

Fig. 1. Differential microscopic cross section $I(q)$ as a function of the scattering vector q based on experimental data in Ref. 3 fitted by the piecewise power law, the Guinier-Porod model, and a power law for very low q. Also, the theoretical $I(q)$ calculated with Eq. (9), R = 2.5 nm, and the radii distribution from Ref. 10 are shown.

The constants B, C, and Q_2 are determined by imposing the continuity of $I(q)$ and its derivative. More information on their values can be found in Ref. 17. The function is multiplied by a global scaling factor A, which further accounts for the conversion to microscopic cross section. The fit result with $Q_1 = 0.016\text{Å}^{-1}$ is shown in Fig. 1. A value of $s = 1.5$ suggests the shape of the diamond nanoparticle is in between rods and platelets.[17] This is in contradiction to the known quasisphericity of the NDs, showing the limitations of these empirical models for a real system. However, the estimation of the ND radius from the fitted R_g gives a value between 2.5 and 5 nm. We consider this result close enough to the average diameter of 5.1 nm (3.1 nm full width at half maximum) reported in Ref. 3. A deeper analysis of the average ND size was conducted in the same paper and is out of the scope of this work.

Even though Eq. (2) has an analytical solution for the Guinier-Porod model, adding the very-low-q power law makes Eq. (4) not integrable when $p \geq 2$. For practical reasons, we opted for numerical integration to solve the problem of evaluating Eq. (2) down to a user-selected value Q_{min}; below this value, a constant $I(q) = I(Q_{min})$ is assumed. This assumption is consistent with the SANS theory.[18] The choice of Q_{min} strongly affects the value of the cross section due to the fast increase in $I(q)$ at very low q. Due to the empirical nature of this model, a suitable choice cannot be taken a priori, but should be guided by the result it yields. We opted to fit the cross-section measurements in Fig. 2. An optimal value was found to be $Q_{min} = 0.05\text{Å}^{-1}$, which is larger then $Q_1 = 0.016\text{Å}^{-1}$. This means that the power-law contribution is in practice not included.

II.C. User-Specified $I(q)$

To expand the code functionality, the computational tools used for the numerical calculation of the Guinier-Porod model can be used to directly sample experimental $I(q)$ from a data file. This option can be particularly useful when the analytical models are insufficient to describe the experimental behavior from special ND samples (e.g., powder mixtures). While custom SANS data could lead to more accurate modeling of the sample in possession, there is evidence of the limitations on the use of these data to samples that are substantially different.[5]

III. THEORETICAL MODEL

The neutron scattering cross section in NDs can be calculated using a hard-sphere model with first Born approximation (HSFBA) to calculate the scattered wave function. A full derivation can be found in the pioneering study by Nesvizhevsky et al.[11] The scattering amplitude from a diamond nanoparticle is given as

$$f(q) = -\frac{2m}{\hbar^2} V_0 R^3 \frac{1}{qR}\left(\frac{\sin(qR)}{(qR)^2} - \frac{\cos(qR)}{qR}\right), \qquad (5)$$

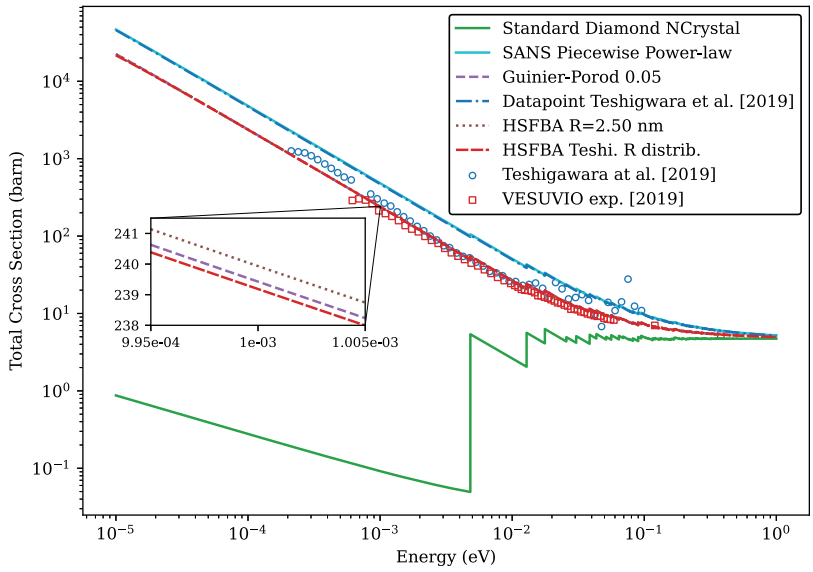

Fig. 2. Total cross section as a function of the neutron energy for ND powder material in NCrystal for a piecewise power law, Gunier-Porod approximation, $I(q)$ data points from Ref. 3, and HSFBA with a fixed radius and radii distribution from Ref. 3 compared to the diamond material in NCrystal[23] and experimental data from Refs. 3 and 15 (only every five points are shown for clarity). The NCrystal kernel for coherent elastic scattering assumes an infinite diamond crystal lattice.

where

m = neutron mass

V = real part of the ND Fermi potential

R = particle size

q = momentum transfer.

The microscopic per-nanoparticle differential cross section is given by $|f(q)|^2$. The calculation of the Fermi potential for a ND powder from its definition (see Eq. (5) in Ref. 11) gives

$$V_0 = \frac{2\pi\hbar^2}{m} b_C n \ , \tag{6}$$

where n is the diamond atomic density and b_C is the carbon coherent scattering length (6.65 fm). If we take 3.53 g/cm^3 as the mass density ρ of diamond inside the nanoparticle, then

$$n = \rho \frac{N_A}{M_C} = 0.177 \text{atoms/Å}^3 \ , \tag{7}$$

where M_C is the carbon molar mass, giving a Fermi potential of 306 neV. Since we are interested in the microscopic per-atom cross section, we need to estimate the number of carbon atoms per nanoparticle by multiplying n by the volume of a sphere-like particle:

$$N_C = \frac{4}{3}\pi n R^3 \ . \tag{8}$$

Finally, substituting Eq. (6) into Eq. (5), taking $|f(q)|^2$, and dividing by N_C, we obtain

$$\frac{d\sigma}{d\Omega}(q) = \frac{16\pi^2 (nb)^2}{N_C} \frac{1}{q^6} (\sin(qR) - qR\cos(qR))^2 \ . \tag{9}$$

This is implemented in NCrystal with R as a user-controlled parameter. The approach used to evaluate σ_{SANS} is once again numerical, even though an analytical solution of Eq. (2) exists. Since a ND powder is more realistically described by a distribution of nanoparticles with different radii, the plugin offers the possibility of passing a file with a list of radii and their respective frequencies. In Fig. 1, we show two comparisons between experimental data from Ref. 3 and the calculation made with both Eq. (9) for a fixed 2.5-nm-radius ND powder and a polydisperse sample using the radii distribution from Ref. 10.

IV. SANSND PLUGIN

From release v2.2.0, NCrystal provides support for plugins to extend existing features, for instance by introducing new or alternative physics models. We implemented the elastic SANS models described in the previous sections to enable users to simulate ND powder samples. The

SANSND plugin is available at the HighNESS repository,[13] and consists mainly of a C++ code and a NCMAT data file. The first one gives instructions to NCrystal on how to evaluate the total cross section for NDs and sample a scattering vector after a collision. The second one is a text file that contains the material information in a format NCrystal can read.

The provided NCMAT file contains both the description of the diamond crystal structure for the elastic bulk physics and the density of states (DOSs) from Ref. 19 for the inelastic component. NCrystal (since v2.0.0) can expand the DOSs to a scattering kernel using the Sjolander method[20] and sample it.[21] The NCMAT file also contains a custom section to pass the chosen SANS model and the parameters as inputs to the plugin. An overview of the models and the parameters is given in Table I.

IV.A. Cross-Section Computation

Sampling from a generic distribution can be easily achieved in NCrystal thanks to several utilities, mainly collected in the classes `PointwiseDist` and `IofQHelper`.[22] First of all, we generate an array of q values that define the range of the distribution; then another array stores the information on $I(q)$ according to the chosen distribution. Initializing an `IofQHelper` object by passing the two arrays will make available the method `calcQIofQIntegral` (E_0), which evaluates the integral in Eq. (2) as $\mathrm{CDF}(k_0)\cdot\int_0^{2k_{max}} qI(q)\mathrm{d}q$, where CDF as a function of k is the cumulative density function (CDF) stored as variable in the initialization phase.

IV.B. Scattering Event Sampling

The cross section as a function of k_0 is used by NCrystal to compute the macroscopic total cross section and sample the distance to the next collision. After a collision, the code randomly picks the reaction based on the ratio of its specific cross section to the total cross section. In the case of SANS, there is no energy exchange, so only the direction after the collision needs to be sampled. Such a task is accomplished by evaluating the cumulative probability distribution

$$\mathrm{CDF}(k_0,q)=\frac{1}{\sigma_{\mathrm{SANS}}(k_0)}\frac{2\pi}{k_0^2}\int_0^q \overline{q}I(\overline{q})d\,\overline{q}\quad , \tag{10}$$

or equivalently,

$$\mathrm{CDF}(k_0,q)=\frac{\int_0^q \overline{q}I(\overline{q})d\,\overline{q}}{\int_0^{2k_0}\overline{q}I(\overline{q})d\,\overline{q}}\quad . \tag{11}$$

The sampled Q is obtained by numerically evaluating the inverse cumulative function $\mathrm{CDF}^{-1}(\xi)$ at a random number $\xi\sim U(0,1)$. In the case of the piecewise power-law model, it is possible to compute analytically the CDF from Eq. (10).

V. VALIDATION

The first step of the validation process is to compare the total cross section for ND powder calculated by NCrystal with the experimental values available in the literature.[3,15] The cross section comparison plot in Fig. 2 shows good agreement with the experimental data for the Gunier-Porod and hard-sphere models. The only noticeable deviations can be seen between 1×10^{-2} and 1×10^{-3} eV, where the Teshigawara experimental data fluctuate with high uncertainty (error bars, here omitted for clarity, are available in Fig. 8 in Ref. 3). At this point, it should also be noted that the NCrystal scattering kernel of the diamond crystal lattice does not include the effects of the finite particle size of the NDs.

The differences observed for the piecewise power-law model and the input of data points can be explained by the high $I(q)$ contribution at very low q, which has

TABLE I

Overview of the Models Available for the NCrystal SANSND Plugin for Version 2.0 with the Respective Parameters

Model	Input Name	Input Parameters
Piecewise power law	PPF	A_1 b_1 A_2 b_2 Q_0
Guinier-Porod + power law	GPF	A s r_g m p Q_{min} Q_1[a]
User-specified $I(q)$	FILE	filename
HSFBA	HSFBA	R in nm or R distribution filename

[a]Optional parameter.

the effect of increasing the total cross section. The multiplication by q in Eq. (2) moderates this effect at very low q, so even though the piecewise power law $I(q)$ diverges at $q = 0$, it yields the same result as the pointwise distribution. As a result, these two models give SANS cross sections ≈ 2 times higher than measured.[3,15] This shows the limitation of including very-low-q SANS contributions and the importance of the Q_{min} parameter in the empirical Guinier-Porod model.

V.A. Backward Reflection Experiment

The experiment chosen as the first validation for the plugin was conducted by Nesvizhevsky et al.[9] in 2008. The experiment was meant to study the scattering of VCNs on powders of NDs with a transmission measurement setup, and in accordance with the model of independent nanoparticles at rest,[11] very intense VCN scattering was observed for the first time. We modeled the experiment in McStas using a monochromatic neutron beam impinging on a sample, 40 × 40 mm and variable thicknesses, defined with the `NCrystal_sample` component and by using the appropriate packing factor to yield a density of 0.6 g cm^3. The detectors, arranged according to the geometry in Fig. 3, were neutron counters with flat entrance windows of 17 × 8 cm arranged along the 11 sides of a regular 12-sided prism. The distance between the sample and the counter was equal to 15 cm. The solid angle coverage was close to 45%. In McStas, the detectors are ideal monitors that track the neutron intensity across the surface. The neutron backward detection probability of the sample is defined as

$$R = \frac{\mathbb{I}\,(120^\circ + 150^\circ + 210^\circ + 240^\circ)}{\mathbb{I}_{TOT}} \quad , \qquad (12)$$

where $\mathbb{I}$ is the sum of detected neutron intensities at the backward monitors, while $\mathbb{I}_{TOT}$ is the total intensity impinging on the target. The forward detection probability is defined similarly by substituting the four forward detectors.

Figure 4 shows a comparison between the curve of a 0.4-mm sample calculated by McStas + plugin + NCrystal and the experimental data. The agreement between the curves is encouraging, but in the comparison with detection probability for the 6-mm sample (Fig. 4b), the model deviates from the experimental data. Our simulation does not include the contribution of absorption and upscatter from the impurities on the surface of the NDs, which becomes important for the thicker sample. Already, Nesvizhevsky and collaborators have noted that by adding this contribution, the performance of the theoretical approach is improved. Since the absorption due to contamination is not taken into account, our material corresponds to pure NDs.

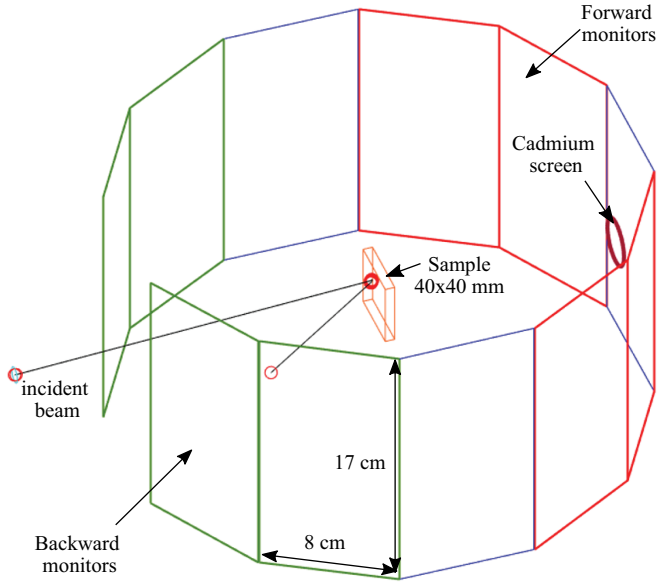

Fig. 3. Scheme of the simulated Nesvizhevsky at al. measurements of backward reflection.[9]

V.B. Reflectometry Experiment

The second validation is meant to test the property of the ND powder to quasispecularly reflect CNs at small angles. The measurement was carried out at the D17 reflectometer at Institut Laue-Langevin, and it is reported in detail in Ref. 2. In Fig. 5, the setup is shown. In Fig. 6, we compare the probability of neutron scattering from the surface of fluorinated detonated nanodiamond (F-DND) powders as a function of the neutron wavelength and the scattering angle for incident neutrons at an angle of $\alpha = 1$ deg. As pointed out in Ref. 2, fluorination consists of a chemical treatment that removes H from DNDs and sharpens the nanoparticle form with the effect of increasing the efficiency of neutron reflection.

Since our plugin simulates pure-carbon NDs, we decided to compare our results with the F-DND sets of data.[2] We normalized the data to the total intensity of the neutron beam hitting the Position Sensitive Detector monitor for each wavelength. The experimental plot in Fig. 6b, normalized in the same way, has a sharp vertical line at $\beta = 1$ deg, which corresponds to the specular reflection of neutrons from the surface of the thin Si window of the sample's container. Since all

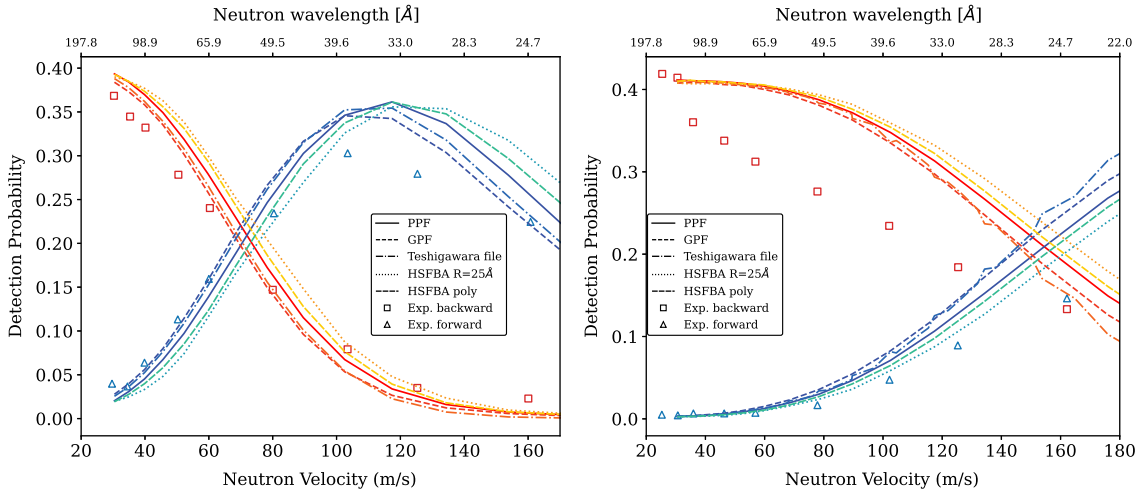

Fig. 4. Detection probability for backward scatter on a (a) 0.4-mm and (b) 6-mm ND sample. The squares are the measured points for the backward reflection, while the triangles are for forward reflection. Different models are represented with lines.

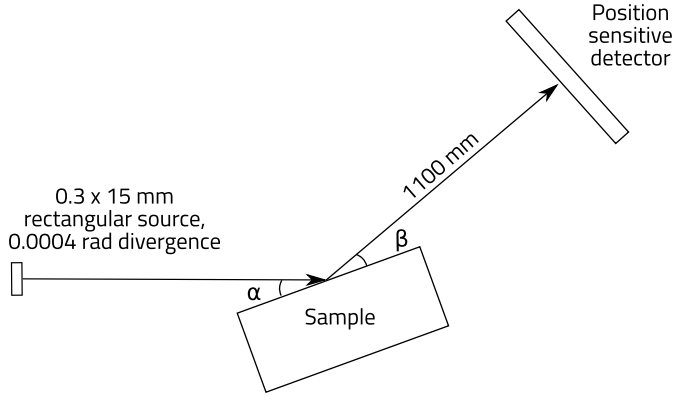

Fig. 5. Side-view scheme of the simulated Nesvizhevsky at al. measurements of quasispecular reflection at the D17 instrument at the ILL (Ref. 2). The two-dimensional position-sensitive ^{3}He detector is 44 cm vertically and 33 cm horizontally.

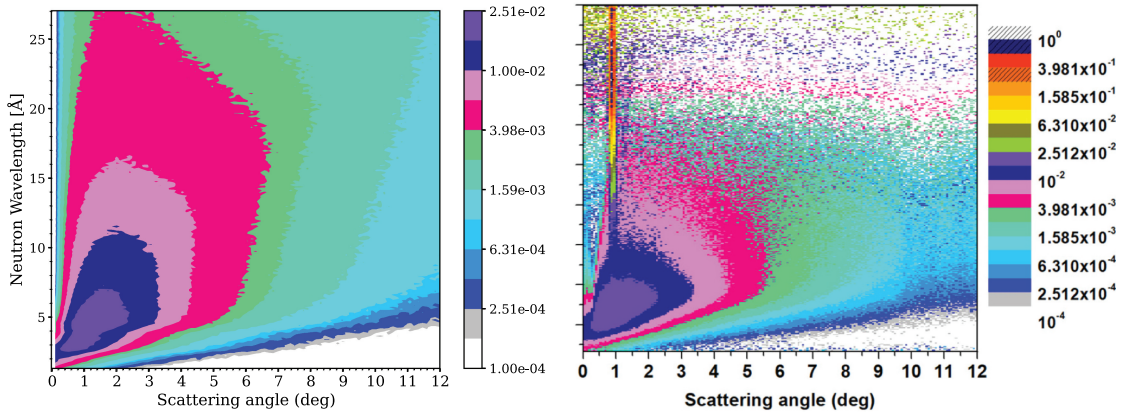

Fig. 6. Probability of neutron scattering from the surface of F-DND powders as a function of the neutron wavelength and the scattering angle in our simulation with (a) the hard-sphere model and (b) in Ref. 2. The neutron incidence angle α is 1 deg.

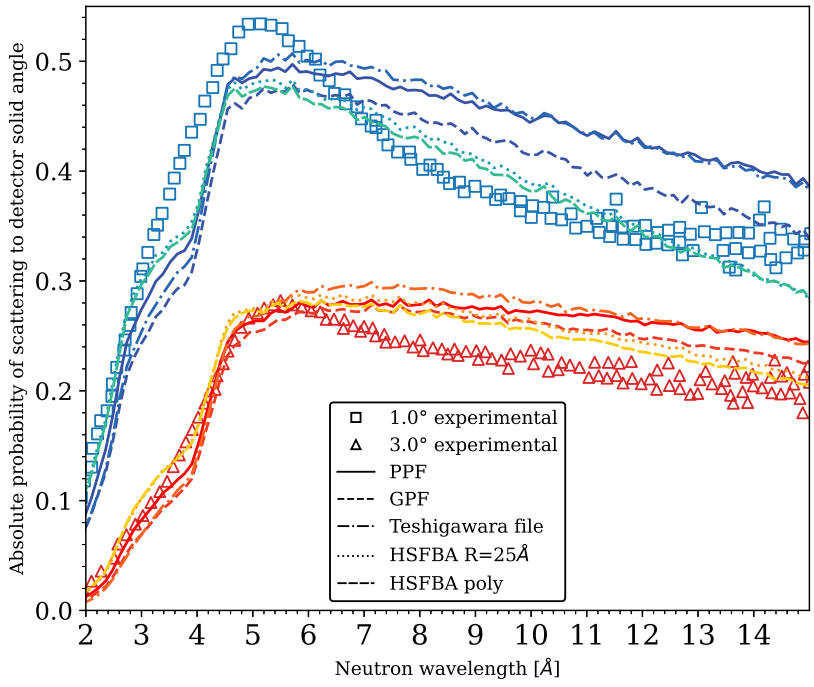

Fig. 7. Absolute probability of neutron scattering to the detector solid angle measured as a function of the neutron wavelength from different inclinations α of the ND sample. The data were integrated over the vertical scattering angle β. The neutron incidence angles α on the sample are 1 and 3 deg. Data from Ref. 2 and the simulated setup in McStas are shown.

subsequent data are corrected for it, we decided for simplicity not to implement any Si window. Moreover, the color binning between the labels in Fig. 6b is assumed to be linear, so small differences in the binning may arise when compared to Fig. 6a. The main patterns, the average spread of the scattering angles, and the probability values are reproduced to a good degree.

In Fig. 7, we compare the absolute probabilities of scattering to the detector solid angle as a function of the neutron wavelength for different α. These curves were obtained from Fig. 6a by integrating in the scattering angle β (or vertical dimension of the detector). So, each point in Fig. 7 is the result of the integration of overall β, while the two sets of curves refer to α angles equal to 1 and 3 deg. The agreement between the experiment and the simulated setup is better for higher α, but overall it is satisfying. In particular, our simulated ND powder seems to capture important features of the curve. The reflectivity efficiency is low at a short wavelength due to large-angle diffraction on the diamond cores, rises, and then decreases at longer wavelengths due to the finite size of the detector.[2] However, experimental data do not show a jump in the reflectivity around 4. This is most likely due to the lack of a small diamond grain model in NCrystal that would broaden the Bragg edge and smear the reflectivity curve.

VI. CONCLUSIONS

We developed a plugin for NCrystal to simulate SANS from ND powder. We calculated the elastic coherent cross section in the low-q range using empirical and theoretical models and validated it against experimental data in the literature.

Validation against reflectivity experiments with McStas simulations further confirmed the good performance of our implementation in modeling neutron scattering for CNs and VCNs. In particular, our simulated ND powder seems to capture important features of the real material, despite the lack of more sophisticated physics, like a model for small diamond grains. This work is part of a wider effort to achieve fast and reliable simulation tools for the design of a beam extraction system for a future VCN source at the ESS. For this reason, a future in-depth study on the enhancing reflective properties of NDs in VCN transport is foreseen.

Disclosure Statement

No potential conflict of interest was reported by the authors.

Funding

This work was funded by the HighNESS project at the ESS. HighNESS is funded by the European Framework for Research and Innovation Horizon 2020 under grant agreement 951782.

ORCID

Nicola Rizzi http://orcid.org/0000-0003-1542-1695
Jose I. Marquez Damian http://orcid.org/0000-0002-9611-914X
Thomas Kittelmann http://orcid.org/0000-0002-7396-4922
Bent Lauritzen http://orcid.org/0000-0001-7173-1650
Esben Klinkby http://orcid.org/0000-0002-1908-5644
Valentina Santoro http://orcid.org/0000-0001-5379-8771

References

1. V. NESVIZHEVSKY et al., "Fluorinated Nanodiamonds as Unique Neutron Reflector," *Carbon*, **130**, 799 (2018); https://doi.org/10.1016/j.carbon.2018.01.086.
2. V. NESVIZHEVSKY et al., "Effect of Nanodiamond Fluorination on the Efficiency of Quasispecular Reflection of Cold Neutrons," *Phys. Rev. A.*, **97**, *2*, 023629 (2018); https://doi.org/10.1103/PhysRevA.97.023629.
3. M. TESHIGAWARA et al., "Measurement of Neutron Scattering Cross Section of Nano-Diamond with Particle Diameter of Approximately 5 nm in Energy Range of 0.2 meV to 100 meV," *Nucl. Instrum. Methods Phys. Res., Sect. A*, **929**, 113 (2019); https://doi.org/10.1016/j.nima.2019.03.038.
4. T. ERSEZ et al., "Small Angle and Inelastic Scattering Investigation of Nanodiamonds," *Physica B*, **551**, 278 (2018); https://doi.org/10.1016/j.physb.2018.04.027.
5. K. GRAMMER and F. GALLMEIER, "The Small-Angle Neutron Scattering Extension in MCNPX and the SANS Cross Section for Nanodiamonds," *Nucl. Instrum. Methods Phys. Res., Sect. A*, **953**, 163226 (2020); https://doi.org/10.1016/j.nima.2019.163226.
6. J. GRANADA, J. DAMIÁN, and C. HELMAN, "Studies on Reflector Materials for Cold Neutrons," *EPJ Web Conf.*, **231**, 04002 (2020); https://doi.org/10.1051/epj-conf/202023104002.
7. M. JAMALIPOUR et al., "Improved Beam Extraction at Compact Neutron Sources Using Diamonds Nanoparticles and Supermirrors," *Nucl. Instrum. Methods Phys. Res., Sect. A*, **1033**, 166719 (2022); https://doi.org/10.1016/j.nima.2022.166719.
8. N. GREINER et al., "Diamonds in Detonation Soot," *Nature*, **333**, *6172*, 440 (1988); https://doi.org/10.1038/333440a0.
9. V. NESVIZHEVSKY et al., "The Reflection of Very Cold Neutrons from Diamond Powder Nanoparticles," *Nucl. Instrum. Methods Phys. Res., Sect. A*, **595**, *3*, 631 (2008); https://doi.org/10.1016/j.nima.2008.07.149.
10. A. ALEKSENSKII et al., "Clustering of Diamond Nanoparticles, Fluorination and Efficiency of Slow Neutron Reflectors," *Nanomaterials*, **11**, *8*, 1945 (2021); https://doi.org/10.3390/nano11081945.
11. V. NESVIZHEVSKY, G. PIGNOL, and K. PROTASOV, "Nanoparticles as a Possible Moderator for an Ultracold Neutron Source," *International Journal of Nanoscience*, **6**, *6*, 485 (2007); https://doi.org/10.1142/S0219581X07005073.
12. X. CAI and T. KITTELMANN, "NCrystal: A Library for Thermal Neutron Transport," *Comput. Phys. Commun.*, **246**, 106851 (2020); https://doi.org/10.1016/j.cpc.2019.07.015.
13. "highness-eu/ncplugin-SANSND"; https://github.com/highness-eu/ncplugin-SANSND/.
14. K. LEFMANN and K. NIELSEN, "McStas, a General Software Package for Neutron Ray-Tracing Simulations," *Neutron News*, **10**, *3*, 20 (1999); https://doi.org/10.1080/10448639908233684.
15. J. GRANADA et al., "Development of Neutron Scattering Kernels for Cold Neutron Reflector Materials," arXiv:2103.09145 [physics] (2021); http://arxiv.org/abs/2103.09145.
16. M. AVDEEV et al., "The Spatial Diamond-Graphite Transition in Detonation Nanodiamond as Revealed by Small-Angle Neutron Scattering," *J. Phys.: Condens. Matter*, **25**, *44*, 445001 (2013); https://doi.org/10.1088/0953-8984/25/44/445001.
17. B. HAMMOUDA, "A New Guinier-Porod Model," *J. Appl. Crystallogr.*, **43**, *4*, 716 (2010); https://doi.org/10.1107/S0021889810015773.
18. D. S. SIVIA, *Elementary Scattering Theory: For X-ray and Neutron Users*, Oxford University Press (2011); https://oxford.universitypressscholarship.com/view/10.1093/acprof:oso/9780199228676.001.0001/acprof-9780199228676.
19. J. XIE et al., "High-Pressure Thermal Expansion, Bulk Modulus, and Phonon Structure of Diamond," *Phys. Rev. B*, **60**, 9444 (1999); https://doi.org/10.1103/PhysRevB.60.9444.
20. A. SJOLANDER, "Multi-Phonon Processes in Slow Neutron Scattering by Crystals," University of Uppsala (1958).
21. -X.-X. CAI et al., "Rejection-Based Sampling of Inelastic Neutron Scattering," *J. Comput. Phys.*, **380**, 400 (2019); https://doi.org/10.1016/j.jcp.2018.11.043.
22. "NCrystal"; https://github.com/mctools/ncrystal.
23. "Standard Diamond NCrystal"; https://github.com/mctools/ncrystal/blob/master/data/C_sg227_Diamond.ncmat.